Convex Optimization of Low Observability Hypersonic Vehicles

Dan Berkenstock
Dept. of Aeronautics and Astronautics
Stanford University
496 Lomita Mall
Stanford, CA 94305
dberkens@stanford.edu

Juan Alonso
Dept. of Aeronautics and Astronautics
Stanford University
496 Lomita Mall
Stanford, CA 94305
jjalonso@stanford.edu

Laurent Lessard
Dept. of Mechanical and Industrial Engineering
Northeastern University
360 Huntington Avenue
Boston, MA 02115
l.lessard@northeastern.edu

***Abstract*—In this paper, we propose an approach to the conceptual design of high speed aerospace vehicles that addresses the coupled behavior of hypersonic aerodynamics and radar cross section. Our approach employs convex optimization, a branch of optimization theory that guarantees global optima for problems expressed with convex objective functions and constraints, combined with cubic splines as cross sectional representations. We demonstrate the process of creating convex surrogates using piecewise linear functions and apply these objective functions to useful test cases, employing a mixture of convex constraints on geometry. We also provide comparisons on the ability to converge to global optima between this type of convex optimization problem to a nonconvex, sequential quadratic programming solver.**

TABLE OF CONTENTS

1. INTRODUCTION

The field of Aerospace Shape Optimization (ASO) has garnered significant attention over the last 30 years, coupling computational modeling of physical performance with optimization routines that iterate a shape towards improved capabilities.

The simulation of aerodynamic performance has often been achieved through implementation of nonlinear, nonconvex partial differential equations, which themselves must be solved using iterative techniques. The computational cost associated with such methods can limit the practicality of broad searches over high dimensional design spaces. Instead, their benefits are often best seen through the refinement of an existing design to a new, local optimum. This leads to a potential dilemma during the conceptual design stage. Often, in order to achieve performance near the global optimum of a given problem, a relatively similarly performing shape must be known a priori.

Convex optimization [4] has been used in a variety of engineering disciplines, from financial analysis to truss design to development of control algorithms. Convex optimization is frequently encountered in trajectory optimization and control system design of both hypersonic re-entry and air breathing vehicles [5]. However, although convex optimization has been employed in vehicle configuration design [7], its use in the physical design of aerodynamic vehicles has been limited.

The computational design of hypersonic vehicles has become of increasing interest in recent years, due to improved computational capabilities, development of several commercial hypersonic transport vehicles, and the requirement for high speed weapons.

In [1], Eyi et al discuss a general framework for combining aerodynamic and thermal design in a high-fidelity, multidisciplinary environment. Similarly, in [2, 3], Kinney demonstrates the approach of three dimensional shape design using Newtonian flow theory, combined with direct manipulation of surface triangulation.

The remainder of this paper is organized as follows. First, we provide a brief overview of the field of convex optimization. We then proceed to outline an approach which combines linear coefficient shape descriptors with convex, trust region, objective function surrogates to generate an optimum in close proximity to the true global optimum. Next, we derive aerodynamic indicators for hypersonic aerodynamics and radar cross section and generate convex surrogates for each. Finally, we demonstrate the proposed method on several vehicle designs, showing the Pareto front of performance tradeoff between hypersonic drag and radar cross section.

2. CONVEXITY ASSISTED SHAPE OPTIMIZATION

In Aerospace Shape Optimization (ASO), the objective is to optimize one, or multiple, measures characterizing performance of a physical vehicle, subject to a set of constraints on the vehicle's geometry and performance. Formally, we seek

978-1-6654-9032-0/23/$31.00

to solve problems of the type

$$\begin{aligned} \underset{z\in D}{\text{minimize}} \quad & f_0(z) \\ \text{subject to} \quad & f_i(z) \leq 0, \quad i = 1, \ldots, m, \end{aligned} \tag{1}$$

where $z \in D$ is a vector of design variables describing the shape of the vehicle and $D \subseteq \mathbb{R}^n$ is the admissible set of variables. In a typical ASO problem, the functions, f_i, may be quite general. For example, they often arise from the discretization of highly non-linear partial differential equations. In general, the objective and constraint functions may be nonlinear, nonconvex, and solved themselves by computationally expensive iterative methods. Additionally, the methods for describing the shape under consideration are varied. Shapes may be defined discretely, by vertices and connectivity, or continuously by polynomials and/or splines that may be explicit or implicit. The solution of problems such as shown in Eq. (1) may be approached locally or globally. Global methods typically involve searching algorithms such as genetic algorithms, particle swarms, or simulated annealing. These methods offer the attractive promise of global optimality, however, they come at a computational cost that can be prohibitive for all but the simplest of problems. Local methods typically iterate an initial solution towards a locally optimal solution by incorporating gradients and, potentially, Hessians. Using adjoint formulations and automatic differentiation techniques, it is computationally tractable to attempt local, gradient-based optimization even with complex vehicle representations and high-fidelity physical models. However, gradient-based optimization of even relatively simple problems can prove exceedingly frustrating for the designer, due to the dependency of the final solution on the quality of the initial guess. In practice, the solution must be repeated many times, starting from differing initial points across the design space, and tuning various parameters of the optimizer. Especially for design spaces of high dimension, it may not be clear to the designer whether anything approaching a global optimum has been achieved.

Conversely, in a convex optimization problem, we add the stipulation that the $f_i : D \to \mathbb{R}$ are *strictly convex*, which means that for all $0 \leq \theta \leq 1$ and $y, z \in D$ with $y \neq z$,

$$\begin{aligned} &\theta y + (1-\theta)z \in D \quad (D \text{ is a convex set}), \text{ and} \\ &f(\theta y + (1-\theta)z) < \theta f(y) + (1-\theta) f(z). \end{aligned}$$

The primary benefit of strictly convex optimization models are 1) they have a global optimum that can be found in polynomial time, 2) no special initialization is typically required, and 3) there exists a rich set of off-the-shelf solvers that require limited expertise for implementation [12, 13]. The primary drawback is the fact that very few governing equations of the underlying physics of useful problems are strictly convex.

The fundamental distinction of this approach is an analysis of the convexity of the underlying objective and constraint functions, which provide a high degree of certainty regarding the quality that should be expected in a final answer. Indeed, there are additional categories of problems that also analyze the nature of the underlying objective and constraint equations and provide some, though less than the strictly convex case, certifications towards global optimality. These include quasiconvex and polynomial optimation. There are also heuristic methods, developed based on principles from convex optimization, which in practice provide solutions to nearly convex problems that are often near the underlying global optimum.

In this work, we propose a combination of these principles we call *Convexity Assisted Shape Optimization* (CASO). There are fundamentally two observations that underly CASO. First, a rich variety of shapes may be represented by explicit polynomial splines with linear coefficients. These lend themselves easily to specification of geometric constraints, including thickness, area, slope, curvature, etc. The second observation is there exist approaches to modelling physical phenomena, of low to medium fidelity, that are either 1) convex, 2) nearly convex, or 3) convex over a trust region within which other information indicates the global solution should lie.

The simplest implementation of CASO is as follows. First, define a physical shape using explicit polynomial splines, with the linear coefficients as design variables. Second, identify the convex trust regions of any relevant physical phenomena. Third, develop convex surrogates for each physical phenomena by taking the maximum of a set of sampled piecewise linear functions. Fourth, combine the menu of constraints and objective functions above to develop and solve convex optimization problems resulting in globally optimal shapes.

While beyond the scope of the current paper, in future research we plan to also describe options to extend this method to the case where the objective function components are nearly, but not strictly, convex or where a transformation may introduce a convex objective function, with the additional of potentially nonconvex constraints.

The specific design problem we consider in the present work is a Multidisciplinary Design Optimization problem whereby we simultaneously seek to minimize the drag and radar cross section of an aerodynamic vehicle subjected to a hypersonic ($M > 5$) flow.

In our case study, we found that using CASO quickly provided useful results, which were only matched by painstakingly tuning generic, gradient based approaches through the execution of hundreds of equivalent problems.

3. AERODYNAMIC PERFORMANCE

In the conceptual design of hypersonic vehicles, it is typical to employ the so-called Newton sine-squared law for estimating the surface pressure coefficient [9]. Under this model, the pressure coefficient is assumed proportional to the squared inner product of the free stream velocity and the local surface normal, so for the portion of the surface impinged by the flow,

$$c_p = 2(\hat{v} \cdot \hat{n})^2. \tag{2}$$

Note that $c_p = 0$ in regions where the flow is blocked by another portion of the body. The normal and axial force imparted to the body may then be integrated such that

$$\begin{aligned} c_n &= \int_0^c (c_{p_l} - c_{p_u})\, \mathrm{d}x \\ c_a &= \int_0^c \left(c_{p_l} \frac{\mathrm{d}y_l}{\mathrm{d}x} - c_{p_u} \frac{\mathrm{d}y_u}{\mathrm{d}x} \right) \mathrm{d}x, \end{aligned} \tag{3}$$

and the lift and drag sectional coefficients are obtained as

$$\begin{aligned} c_l &= c_n \cos\alpha - c_a \sin\alpha \\ c_d &= c_n \sin\alpha + c_a \cos\alpha. \end{aligned} \tag{4}$$

Due to the difficulty of obtaining analytic integrals for complex shapes, it is customary to discretize the body into a series of simpler constituent panels, often linear segments. We shall assume sampling at fixed intervals along the x axis, with integration beginning at the trailing edge and proceeding in a clockwise fashion. Furthermore, for illustrative purposes we will assume zero angle of attack, so that the lift and normal force vectors are aligned as well as the drag and axial force vectors. In this case,

$$c_l = c_n = 2\left(\sum_{i=0}^{n/2}\frac{\Delta y_i^2\Delta x}{\Delta y_i^2+\Delta x^2} - \sum_{n/2+1}^{n-1}\frac{\Delta y_i^2\Delta x}{\Delta y_i^2+\Delta x^2}\right)$$
$$c_d = c_a = 2\left(\sum_{i=0}^{n/2}\frac{\Delta y_i^3}{\Delta y_i^2+\Delta x^2} + \sum_{n/2+1}^{n-1}\frac{\Delta y_i^3}{\Delta y_i^2+\Delta x^2}\right), \tag{5}$$

where $\Delta y_i = y_{i+1} - y_i$ and Δx is a constant. Note that for zero angle of attack and for a convex body, the impinged section of the surface will have $\Delta y_i \geq 0$, while $\Delta x \leq 0$ and $\Delta x \geq 0$ for the lower and upper surfaces, respectively.

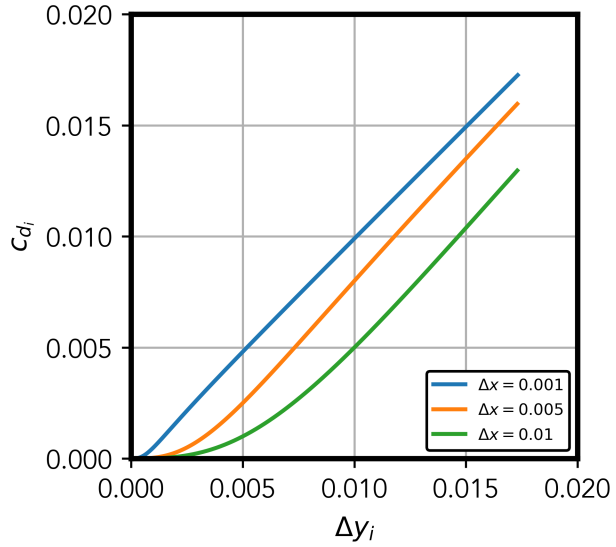

Figure 1. Drag coefficient as function of Δy_i.

4. Electromagnetic Performance

The Stratton-Chu integrals are solutions to Maxwell's equations, which express the radiated energy at a point in space [10, 11]. In this case, they will describe the electrical wave induced by a set of currents present on a body, which themselves have been induced by a radar wave. As presented by Jenn [10], the radar cross section is given as,

$$\sigma = \lim_{r\to\infty} 4\pi r^2 \frac{|\vec{E}(r,\theta,\phi)|^2}{|\vec{E}_i|^2}, \tag{6}$$

where, the electric field observed at a point is given as,

$$\vec{E}(r,\theta,\phi) = \frac{-jk\eta}{4\pi r}\iiint_V \vec{J}e^{jkg}\,\mathrm{d}v', \tag{7}$$

The physical optics approximation for the body currents, $\vec{J}$, are applicable for electrically large bodies. On the illuminated portion of the body,

$$\vec{J} = 2\hat{n}\times\vec{H}_i, \tag{8}$$

and $\vec{J} = 0$ elsewhere. Consider an incident wave, where, for the two dimensional case,

$$\vec{E}_i = E_{0\theta}e^{-j\vec{k}_i\cdot\vec{r}}\hat{\theta} \tag{9}$$

As in the case of hypersonic aerodynamics, we discretize a body into a set of linear segments. Completing the integration above, for a single panel, results in,

$$E(r,\theta) = \frac{-je^{-jkr}E_{0\theta}}{2\pi r}h_i\,\mathrm{sinc}(k(\Delta x\cos\theta + \Delta y_i\sin\theta)), \tag{10}$$

where, $h_i = (-\Delta x\sin\theta + \Delta y_i\cos\theta)$. Evaluating the limit, the resulting radar cross section for an individual panel, is given as,

$$\sigma_i = \frac{4\pi}{\lambda^2}h_i^2\,\mathrm{sinc}(k(\Delta x\cos\theta + \Delta y_i\sin\theta))^2. \tag{11}$$

For conceptual design purposes, we proceed to use the geometrical components method, adding the contributions from each component noncoherently, such that,

$$\sigma = \sum_i \sigma_i. \tag{12}$$

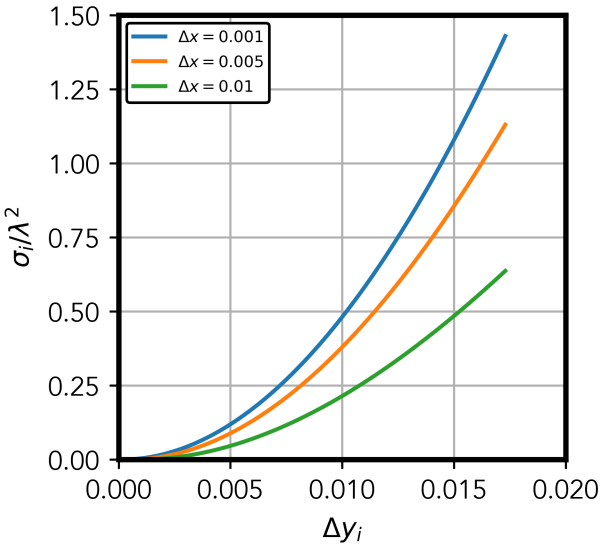

Figure 2. RCS as function of Δy_i, ($\theta = 5°$,$\lambda = 0.05$m).

5. CASO Implementation

We will now demonstrate an implementation of CASO using the method outlined above. First, we define the vehicle cross section using cubic splines for both the top and bottom surfaces. Second, we analyze the functions for drag and radar cross section and develop convex surrogates for each. Finally, we will combine the objective function with a menu of geometric constraints to develop solvable convex optimization problems.

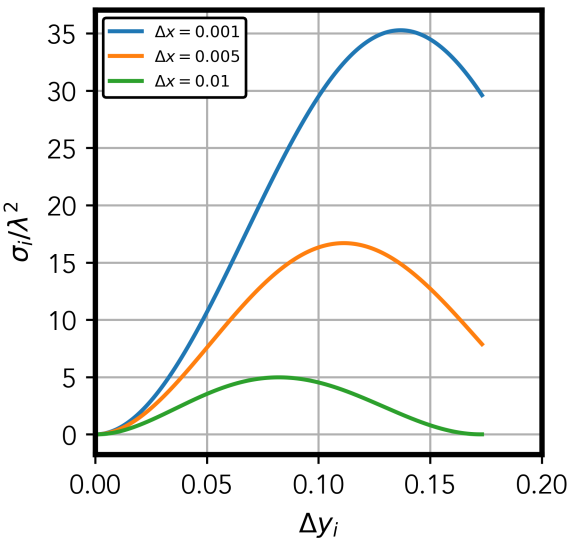

Figure 3. **RCS as function of Δy_i, ($\theta = 5°$,$\lambda = 0.05$m).**

Shape Representation and Geometric Constraints

For simplicity, we derive relevant equations for the two-dimensional case (designing a vehicle cross-section), but it is straightforward to generalize our methods to three dimensions. A variety of parameterizations may be used to describe the shape of the vehicle, such as arbitrary combinations of piecewise basis functions. However, for this approach it is important that explicit shape definitions are used, i.e. the vehicle is described as $y(x)$, not $[x(t) \quad y(t)]$. Again for simplicity of exposition, we will use *cubic splines* to parameterize the upper and lower surfaces of the cross-section. In this section, we will derive the necessary mathematics for cubic spline parameterizations and provide a menu of applicable geometric constraints for use in design problems.

Cubic Spline Representation—A cubic spline is a continuous piecewise function where each piece is a cubic polynomial. The points where successive polynomials are stitched together are called *knots*. At each knot, the adjacent cubics are constrained to have matching position, slope and curvature (first and second derivative).

The i^{th} polynomial, for $x_{\text{knot}_i} \leq x \leq x_{\text{knot}_{i+1}}$ has the form

$$y_i(x) = a_i x^3 + b_i x^2 + c_i x + d_i,$$

and, at each knot, $x = x_{\text{knot}_i}$, the matching conditions are

$$\begin{aligned} a_i x^3 + b_i x^2 + c_i x + d_i &= a_{i+1} x^3 + b_{i+1} x^2 + c_{i+1} x + d_{i+1} \\ 3a_i x^2 + 2b_i x + c_i &= 3a_{i+1} x^2 + 2b_{i+1} x + c_{i+1} \\ 6a_i x + 2b_i &= 6a_{i+1} x + 2b_{i+1}. \end{aligned}$$

In representing a vehicle cross section, we employ separate splines, $y_u(x)$ and $y_l(x)$ with $0 \leq x \leq 1$ for the upper and lower surfaces, where we adopt the following notation for each polynomial:

$$\begin{aligned} y_{u_i}(x) &= a_{u_i} x^3 + b_{u_i} x^2 + c_{u_i} x + d_{u_i}, \\ y_{l_i}(x) &= a_{l_i} x^3 + b_{l_i} x^2 + c_{l_i} x + d_{l_i}. \end{aligned}$$

Here, we elect to use two segments for the top and bottom splines, with fixed knots located at x_{knot}, resulting in a sixteen-dimensional design space. We further constrain the upper and lower splines to meet on the x-axis at the leading and trailing edges of the cross-section, giving the four constraints

$$\begin{aligned} d_{u_0} &= d_{l_0} = 0 \\ a_{u_1} + b_{u_1} + c_{u_1} + d_{u_1} &= 0 \\ a_{l_1} + b_{l_1} + c_{l_1} + d_{l_1} &= 0. \end{aligned} \tag{13}$$

Between the six equations enforcing continuity of position, slope, and curvature at the knot on both splines, and the four equations that fix the leading and trailing edges, six degrees of freedom remain. An illustrative sample of 180 possible shapes generated from this design space are shown in Fig. 4.

Geometric Constraints—As we describe in [8], this explicit, polynomial-based representation lends itself to a number of convex, geometric constraints, including those listed in Table 1.

Table 1. Convex geometric constraints.

Geometric Constraints
Minimum/Maximum thickness
Minimum/Maximum area
Minimum/Maximum slope
Minimum/Maximum curvature
Internal payload constraints
Non-Intersection constraint
Maximum arc length constraint

For example, it is possible to express a maximum thickness, $\tau_{\max}$ constraint by enforcing a maximum distance between the two surfaces over the range, $0 \leq x \leq 1$, such that,

$$\max\left(\tau(\mathrm{x})\right) \leq \tau_{\max}, \tag{14}$$

where,

$$\begin{aligned} \tau(x) = (a_{u_i} - a_{l_i})x^3 + (b_{u_i} - b_{l_i})x^2 \\ + (c_{u_i} - c_{l_i})x + d_{u_i} - d_{l_i}. \end{aligned} \tag{15}$$

As the maximum of an affine set, this represents a convex constraint. Conversely, the minimum thickness over a prescribed region, $x_1 \leq x \leq x_2$, may be enforced as,

$$\min\left(\tau(\mathrm{x})\right) \geq \tau_{\min}. \tag{16}$$

A non-intersection constraint may be created by using this constraint with $x_1 = 0$, $x_2 = 1$, and $\tau_{\min} = 0$.

Minimum and maximum constraints on slope and curvature may be treated similarly. For the cubic spline described above, the area contained within the vehicle cross section is given by,

$$A = \int_0^{x_{\text{knot}}} (y_{u_0} - y_{l_0})\,\mathrm{d}x + \int_{x_{\text{knot}}}^1 (y_{u_1} - y_{l_1})\,\mathrm{d}x, \tag{17}$$

or

$$\begin{aligned} A =& (a_{u_1} - a_{l_1})\left(\frac{1}{4} - \frac{x_{\text{knot}}^4}{4}\right) + (b_{u_1} - b_{l_1})\left(\frac{1}{3} - \frac{x_{\text{knot}}^3}{3}\right) \\ &+ (c_{u_1} - c_{l_1})\left(\frac{1}{2} - \frac{x_{\text{knot}}^2}{2}\right) + (d_{u_1} - d_{l_1})\left(1 - x_{\text{knot}}\right) \\ &+ \frac{1}{4}(a_{u_0} - a_{l_0})x_{\text{knot}}^4 + \frac{1}{3}(b_{u_0} - b_{l_0})x_{\text{knot}}^3 \\ &+ \frac{1}{2}(c_{u_0} - c_{l_0})x_{\text{knot}}^2 + (d_{u_0} - d_{l_0})x_{\text{knot}} \end{aligned} \tag{18}$$

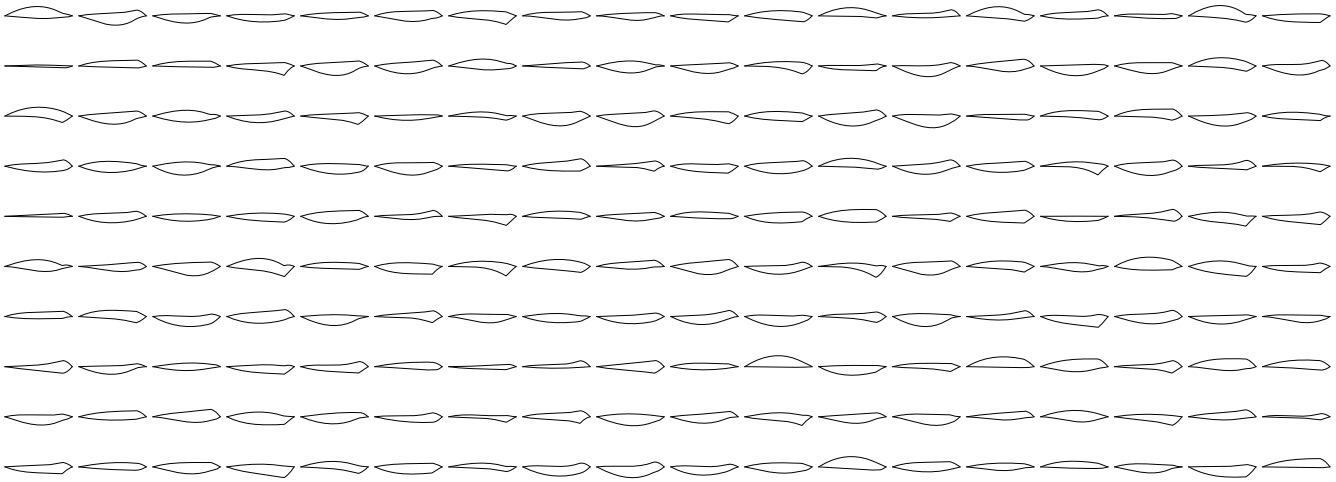

Figure 4. **Illustrative shape instances sampled from the six-dimensional design space described in Section 5.**

which results in an affine expression of the spline coefficients, enabling the convex constraints,

$$A \geq A_{\min} \qquad \text{or} \qquad A \leq A_{\max}. \tag{19}$$

In addition, we note that this approach may be used to ensure that the vehicle design will be large enough to enclose a convex internal payload of given size, such as a circle or square.

Convex Approximations of Performance Indicators

After specifying our approach to shape parameterization and geometric constraints we proceed to analyze the convexity of the aerodynamic and electromagnetic performance measures presented above. In doing so, we will find that they are strictly convex over a trust region within which a globally optimal design is likely to exist. We will then derive *disciplined convex programming* [14] expressions for each performance indicator in order to ease implementation of subsequent optimization problems in readily available convex optimization modeling tools. Although the initial performance indicators are convex over a trust region of interest, they are not globally convex. In order to use common software packages, we will express these functions as the maximum over a set of piecewise linear functions. The resulting surrogates will match the underlying functions exactly over the trust region.

Hypersonic Aerodynamics—Following the methods outlined previously, the vehicle drag coefficient in a hypersonic flow may be modelled as a summation of individual, linear panel contributions, c_{d_i}. The second derivative of this per-panel drag contribution, given in Eq. (4), with respect to Δy is,

$$\frac{\mathrm{d}^2 c_{d_i}}{\mathrm{d}\Delta y^2} = \frac{6\Delta x^4 \Delta y - 2\Delta x^2 \Delta y^3}{\left(\Delta x^2 + \Delta y^2\right)^3}, \tag{20}$$

which is shown for multiple Δx below in Fig. 5. This function has a zero at $\Delta y = \sqrt{3}\Delta x$, and is convex for $\Delta y \leq \sqrt{3}\Delta x$. For present purposes we assume the design of hypersonic vehicles with sharp leading edges, consistent with those that reenter after traversing the upper atmosphere, but not orbital velocities. These vehicles tend to be slender, with a maximum thickness to length ratio much less than unity. The convex region of the per panel drag contribution extends up to a panel inclination of $60°$, a trust region which our design

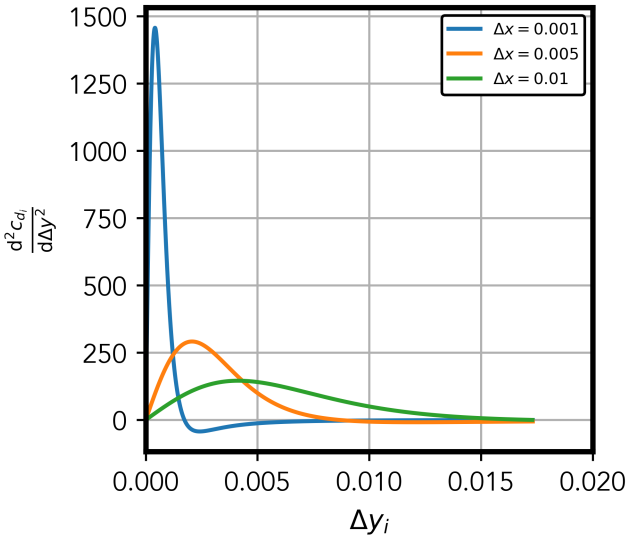

Figure 5. **Curvature of drag coefficient as function of Δy_i.**

studies has shown is more than sufficient to model realistic vehicle shapes.

Examining the case of $\Delta x = .005$, we proceed to derive a disciplined convex expression of c_{d_i} over the range $0 \leq \Delta y \leq \sqrt{3}\Delta x$. We approach this by sampling the value, b_i and derivative, m_i, of the function at a dense number of sample points, Δy_i. We then approximate the function, $c_{d_i}(\Delta y)$ as

$$c_{d_{i,\mathrm{pwl}}}(\Delta y) = \max_{\mathrm{i}}[(\Delta \mathrm{y} - \Delta \mathrm{y_i})\mathrm{m_i} + \mathrm{b_i}] \tag{21}$$

The sampled points and associated slopes and line segments of a dense sampling are shown in Fig. 6. For illustrative purposes, we also show a closer view of the piecewise linear nature of the approximation in Fig. 7, created using a much coarser sampling.

One benefit of the piecewise linear approach is that $c_{d_{i,\mathrm{pwl}}} = 0$ automatically for segments of the vehicle for which $\Delta y_i \leq 0$, corresponding to zero drag contribution from areas of the vehicle's surface which are not impinged by the freestream

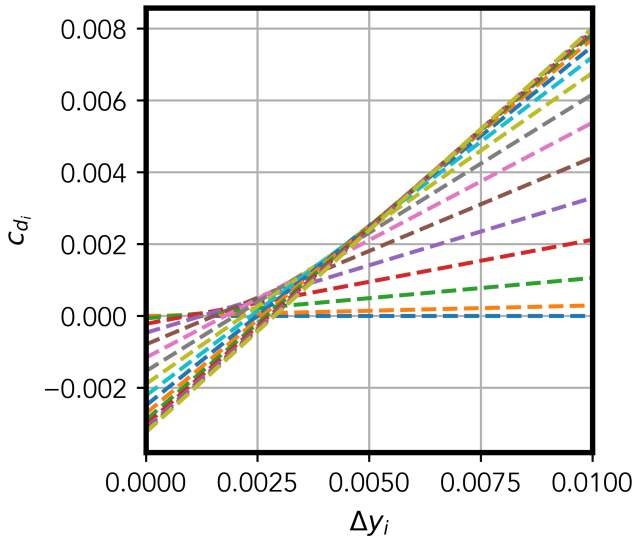

Figure 6. **Set of sampled linear approximations to c_{d_i}.**

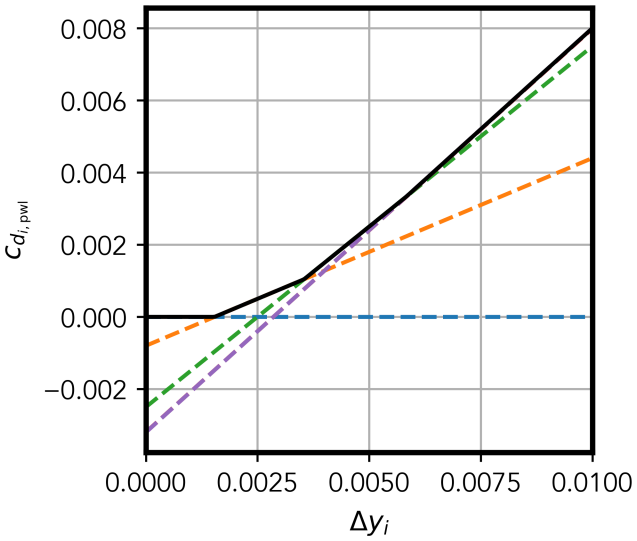

Figure 7. **Coarsely sampled linear approximations to c_{d_i} and piece-wise maximum over the set, $c_{d_{i,\mathrm{pwl}}}$, (shown as solid line).**

flow. Using this fact, the final, approximated drag of the vehicle is given as,

$$c_{d_{\mathrm{pwl}}} = \sum_k \max_{\mathrm{i}}[(\Delta \mathrm{y_k} - \Delta \mathrm{y_i})\mathrm{m_i} + \mathrm{b_i}]. \qquad (22)$$

In the general case, the CASO approach admits the use of non-zero angles of attack and optimization problems involving lift coefficient and/or lift-to-drag ratio. In the current paper, we focus on the case of zero angle of attack drag for illustrative purposes and will develop the mechanisms for extending this approach in a subsequent paper.

Radar Cross Section—The radar cross section variation of a single linear panel, with fixed $\Delta x = 5/1000$ is shown in Fig. 8 for varying monostatic inclination angles, θ.

Based on the high speed ($M_\infty \geq 5$) and high operating altitudes of hypersonic vehicles, by necessity the inclination angle for observation will be quite low, on the order of $\theta =$

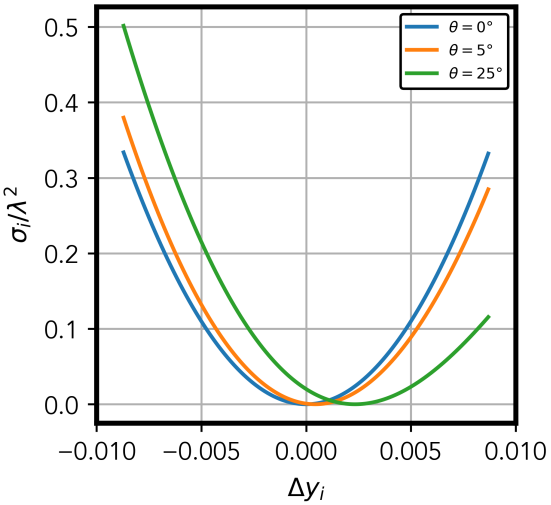

Figure 8. **Monostatic RCS variation ($\lambda = 5cm$).**

$5°$. In addition, long distance radar installations, of the type used to identify such vehicles, often operate wavelengths near $\lambda = 0.05\mathrm{m}$.

Within these operating conditions, the RCS of a single panel is a convex function over the range $0 \leq \Delta y \lessapprox 5.75\sqrt{3}\Delta x$, for $\Delta x = 5/1000$, well beyond the trust region established for the case of hypersonic drag. We again generate a piecewise linear representation for ease of implementation in subsequent optimization problems.

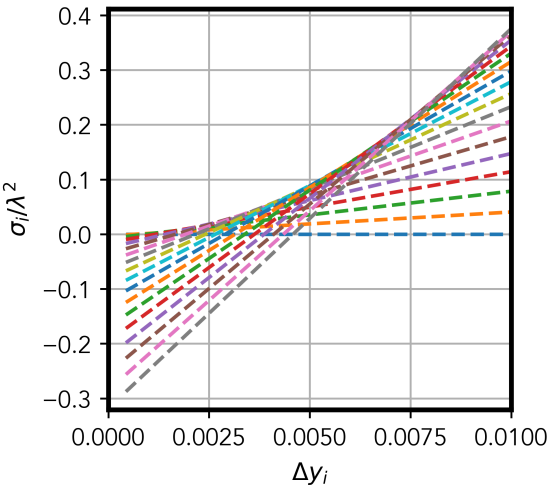

Figure 9. **Set of sampled linear approximations to σ, $\theta = 5°$, top surface.**

Unlike the per panel drag contribution, the panelwise radar cross section contribution is not symmetric about the y-axis, due to the nonzero inclination angle of the monostatic radar wave. This results in separate convex conjugates for the upper and lower surfaces, respectively. On the upper surface, where $\Delta x \geq 0$, the surface is shadowed from the radar wave, and therefore $\sigma_i = 0$, in the case where $\Delta y \geq \Delta x \tan(\theta)$, as shown in Fig. 9. On the bottom surface, where $\Delta x \geq 0$, the surface also is shadowed from the radar wave, and therefore $\sigma_i = 0$, in the case where $\Delta y \geq \Delta x \tan(\theta)$. However, as shown in Fig. 10, this nonzero contribution now extends, unlike drag at zero angle of attack, to slightly negative Δy_i

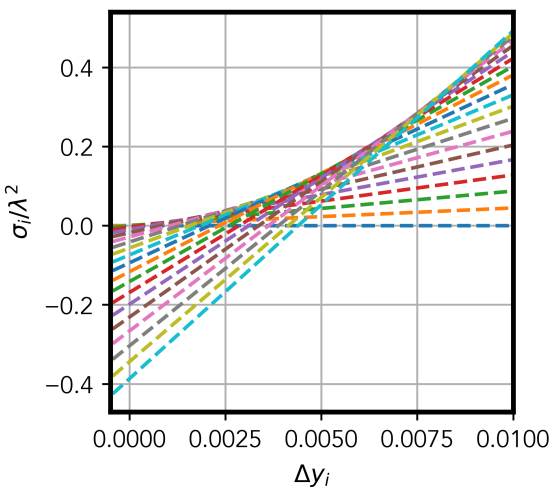

Figure 10. Set of sampled linear approximations to σ, $\theta = 5°$, bottom surface.

values.

As in the case of the drag, we arrive at a final, disciplined convex programming surrogate by summing the panelwise contributions, such that,

$$\begin{aligned}\sigma_{\text{pwl}} = &\sum_{\text{bot}} \max_{\text{i}}[(\Delta \text{y}_{\text{k}} - \Delta \text{y}_{\text{b}_\text{i}})\text{m}_{\text{b}_\text{i}} + \text{b}_{\text{b}_\text{i}}] + \\ &\sum_{\text{top}} \max_{\text{i}}[(\Delta \text{y}_{\text{k}} - \Delta \text{y}_{\text{t}_\text{i}})\text{m}_{\text{t}_\text{i}} + \text{b}_{\text{t}_\text{i}}],\end{aligned} \tag{23}$$

which also automatically ensures $\sigma_i = 0$ in the case where $\Delta y_i \leq \Delta x \tan(\theta)$.

Design Problem Statement

Using the convex approximations derived above, we now proceed to identifying specific optimization problems of interest. In particular, we are interested in problems which minimize a convex combination of hypersonic drag and vehicle radar cross section, while meeting various geometric constraints.

$$\begin{aligned}\underset{z}{\text{minimize}} \quad & \gamma c_{d_{\text{pwl}}} + (1-\gamma)\sigma_{\text{pwl}} \\ \text{subject to} \quad & f_i(z) \leq 0\end{aligned} \tag{24}$$

where the design vector, z contains the sixteen coefficients which define the spline segments of the upper and lower surfaces. The functions f_i are convex functions of the design variables, which enforce geometric constraints on the vehicle.

In the next section, we demonstrate this approach with several case study examples. We then proceed to compare this implementation with a standard gradient based optimizer to show the value of the convex approach.

6. Case Study Examples

In this section, we will consider three examples of optimization problems using this method. In developing these problems, we will consider a sample mission of a hypersonic vehicle traveling at zero angle of attack, $\alpha = 0$, seeking to evade a long-range, monostatic, C-band radar with $\lambda = 0.05m$. We will assume a radar wave incoming at an angle of $\theta = 5°$.

Minimum Drag Subject to RCS and Geometric Constraints

The first example we examine is the problem of minimizing drag subject to a maximum radar cross section and a minimum thickness, $\tau_{\min}$ at a prescribed location, x_c. We therefore state this problem as,

$$\begin{aligned}\underset{z}{\text{minimize}} \quad & c_{d_{\text{pwl}}} \\ \text{subject to} \quad & y_u(x_c) - y_l(x_c) \geq \tau_{\min} \\ & \sigma_{\text{pwl}} \leq \sigma_{\max} \\ & c_{u_0} \geq 0 \\ & c_{l_0} \leq 0 \\ & y_l(0) = y_u(0) = y_l(1) = y_u(1) = 0 \\ & y_{u,l_0}(x_{\text{knot}}) = y_{u,l_1}(x_{\text{knot}}) \\ & y'_{u,l_0}(x_{\text{knot}}) = y'_{u,l_1}(x_{\text{knot}}) \\ & y''_{u,l_0}(x_{\text{knot}}) = y''_{u,l_1}(x_{\text{knot}}),\end{aligned} \tag{25}$$

For the case where $\sigma_{\max} = 0.75$, $x_c = 0.7$ and $\tau_{\min} = .125$, we compute a minimum $c_d = 0.00114$ with an area, $A = 0.0805$. The resulting vehicle cross section is shown below in Fig. 11.

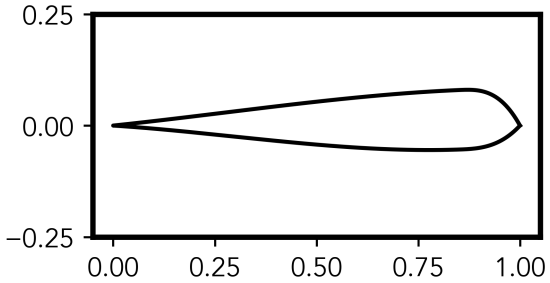

Figure 11. Optimal vehicle cross section: minimum drag subject to maximum RCS constraint.

Optimal Tradeoff Curve: Minimum Area Constraint

The next example we present involves the minimization of a convex combination of drag coefficient and radar cross section along with a small regularization term on the squared third derivative of the spline comprising the vehicle, subject to a minimum area constraint. Formally, we seek to solve the following problem,

$$\begin{aligned}\underset{z}{\text{minimize}} \quad & \gamma c_{d_{\text{pwl}}} + (1-\gamma)\sigma_{\text{pwl}} + \epsilon \left(\sum_i a_{u_i}^2 + a_{l_i}^2 \right) \\ \text{subject to} \quad & A(z) \geq 0.15 \\ & c_{u_0} \geq 0 \\ & c_{l_0} \leq 0 \\ & y_l(0) = y_u(0) = y_l(1) = y_u(1) = 0 \\ & y_{u,l_0}(x_{\text{knot}}) = y_{u,l_1}(x_{\text{knot}}) \\ & y'_{u,l_0}(x_{\text{knot}}) = y'_{u,l_1}(x_{\text{knot}}) \\ & y''_{u,l_0}(x_{\text{knot}}) = y''_{u,l_1}(x_{\text{knot}}),\end{aligned} \tag{26}$$

where $z = [a_{u_i} \quad b_{u_i} \quad c_{u_i} \quad d_{u_i} \quad a_{l_i} \quad b_{l_i} \quad c_{l_i} \quad d_{l_i}]$, for $i \in [0 \quad 1]$. We solve this problem for a variety of values $0 \leq \gamma \leq 1$, and present the ensuing Pareto front below in Fig. 12 and a sampling of vehicle shapes in Fig. 13.

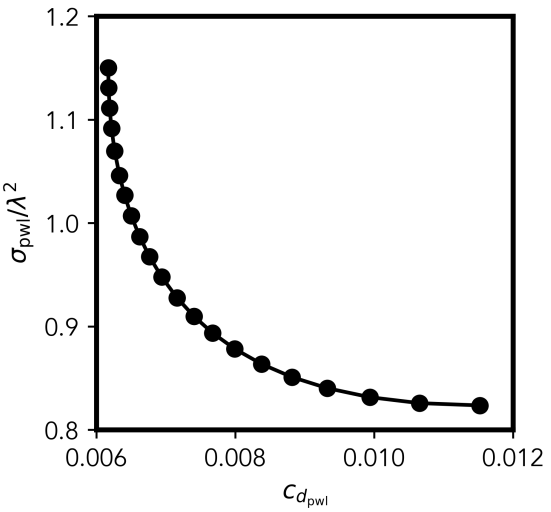

Figure 12. **Optimal tradeoff between drag and radar cross section, $A_{\min} = 0.15$.**

Optimal Tradeoff Curve: Minimum Thickness Constraint

The final example we present again involves the minimization of a convex combination of drag coefficient and radar cross section along with a small regularization term on the squared third derivative of the spline comprising the vehicle. However, in this case we implement a minimum thickness constraint over a prescribed subsection of the vehicle. Therefore, we now seek to solve the following problem,

$$\begin{aligned}
\underset{z}{\text{minimize}} \quad & \gamma c_{d_{\text{pwl}}} + (1-\gamma)\sigma_{\text{pwl}} + \epsilon \left(\sum_i a_{u_i}^2 + a_{l_i}^2 \right) \\
\text{subject to} \quad & \tau(x_1 \leq x \leq x_2) \geq \tau_{\min} \\
& c_{u_0} \geq 0 \\
& c_{l_0} \leq 0 \\
& y_l(0) = y_u(0) = y_l(1) = y_u(1) = 0 \\
& y_{u,l_0}(x_{\text{knot}}) = y_{u,l_1}(x_{\text{knot}}) \\
& y'_{u,l_0}(x_{\text{knot}}) = y'_{u,l_1}(x_{\text{knot}}) \\
& y''_{u,l_0}(x_{\text{knot}}) = y''_{u,l_1}(x_{\text{knot}}), \qquad (27)
\end{aligned}$$

where $z = [a_{u_i} \quad b_{u_i} \quad c_{u_i} \quad d_{u_i} \quad a_{l_i} \quad b_{l_i} \quad c_{l_i} \quad d_{l_i}]$, for $i \in [0 \quad 1]$. We solve this problem for a variety of values $0 \leq \gamma \leq 1$, with $x_1 = 0.6$, $x_2 = 0.8$, and $\tau_{\min} = 0.15$, and present the ensuing Pareto front below in Fig. 14 and a sampling of vehicle shapes in Fig. 15.

7. Optimization Comparisons

As stated previously, convex optimization offers significant benefits for situations where the objective and constraint functions of a problem are convex. Because convex optimization guarantees a global optimum in polynomial time, no initialization point is required for the optimizer. This ensures that problems can be solved accurately and quickly, without the type of tuning that can be required for traditional, nonconvex, gradient based optimizers. Especially when a gradient is not available analytically, there can be significant, and expensive, efforts required to tune the various convergence and finite difference parameters. Below, we show three comparisons running the minimum area case study example using both convex optimization solvers as well as a readily available sequential quadratic programming solver. In each case, we run the gradient-based, SQP solver, from $n = 256$ random starting locations for each value of γ. Although, through trial and error, it is possible to achieve identical results, several orders of magnitude in the finite difference step creates dramatically poorer convergence to the true global optima along the Pareto front. For reference, the convex optimization solutions were created using CVXPY[2], which transforms problems into a standard conic form, which are then solved using MOSEK[3]. The gradient based optimization was performed using MATLAB's fmincon function, with the sequential quadratic programming algorithm and central finite differencing, with stepsize, h. The results are shown below in Figs. 16 to 18.

8. Conclusions

In this paper, we have proposed and implemented a new approach, termed Convexity Assisted Shape Optimation (CASO), for applying convex optimization to multidisciplinary design optimization problems combining hypersonic aerodynamics and radar cross section. We have applied this method to several test cases combining the optimization of drag and radar cross section with geometric constraints, including minimum area and minimum thickness constraints. Finally, we have demonstrated the user benefits of a convex optimization approach, with a significant reduction in time spent tuning optimizer configurations.

References

[1] Sinan Eyi, Kyle M. Hanquist, and Iain D. Boyd. "Aerothermodynamic Design Optimization of Hypersonic Vehicles," Journal of Thermophysics and Heat Transfer, 33:2, 392-406, 2019.

[2] David Kinney. "Aero-Thermodynamics for Conceptual Design," AIAA 2004-31. 42nd AIAA Aerospace Sciences Meeting and Exhibit. January 2004.

[3] David Kinney. "Aerodynamic Shape Optimization of Hypersonic Vehicles," AIAA 2006-239. 44th AIAA Aerospace Sciences Meeting and Exhibit. January 2006.

[4] S. Boyd and L. Vandenberghe, Convex Optimization. Cambridge University Press, 2004.

[5] Binbin Yan, Ruifan Liu, Pei Dai, Muzeng Xing, Shuangxi Liu, "A Rapid Penetration Trajectory Optimization Method for Hypersonic Vehicles", International Journal of Aerospace Engineering, 2019.

[6] Naresh Kumar, G., Ikram, M., Sarkar, A.K. et al. "Hypersonic flight vehicle trajectory optimization using pattern search algorithm". Optim Eng 19, 125–161, 2018.

[7] Warren Hoburg and Pieter Abbeel. "Geometric Programming for Aircraft Design Optimization," AIAA Journal, 52:11, 2414-2426, 2014.

[8] Daniel Berkenstock, Juan J. Alonso and Laurent Lessard. "A Convex Optimization Approach to Thin Airfoil Design," AIAA 2022-3356. AIAA AVIATION 2022 Forum. June 2022.

[9] John D. Anderson, Jr. "Fundamentals of Aerodynamics, 3rd Edition," McGraw-Hill Higher Education, 2001.

[2] www.cvxpy.org
[3] www.mosek.com

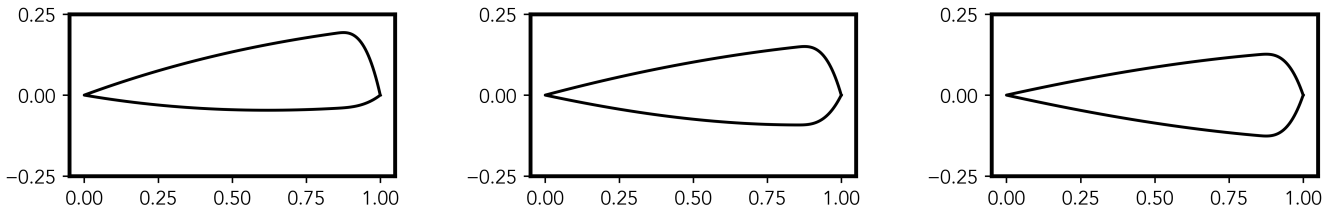

(a) $\gamma = 0.0$ - prioritized rcs reduction (b) $\gamma = 0.5$ - equally prioritized rcs and drag (c) $\gamma = 1.0$ - prioritized drag reduction

Figure 13. Optimal vehicle cross sections (minimum area constraint) for varying γ ($\theta = 5°$, $\alpha = 0°$).

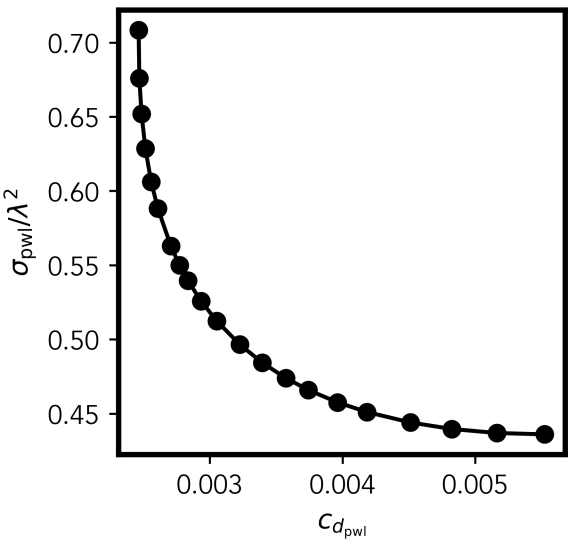

Figure 14. **Optimal tradeoff between drag and radar cross section, $\tau_{\min} = 0.15$.**

[10] David C. Jenn. "Radar and Laser Cross Section Engineering," AIAA education series, American Institute of Aeronautics and Astronautics, 2005.

[11] Eugene F. Knott, John F. Schaeffer and Michael T. Tulley. "Radar Cross Section, 2nd Edition," The Institution of Engineering and Technology, 2004.

[12] S. Diamond and S. Boyd. . "CVXPY: A Python-embedded modeling language for convex optimization," Journal of Machine Learning Research, 17(83):1–5, 2016.

[13] A. Agrawal, R. Verschueren, S. Diamond, and S. Boyd. . "A rewriting system for convex optimization problems," Journal of Control and Decision, 5(1):42–60, 2018.

[14] Michael Grant, Stephen Boyd, and Yinyu Ye. . "Disciplined Convex Programming." In Global Optimization: From Theory to Implementation, edited by Leo Liberti and Nelson Maculan , 115-210. Springer, New York, NY, 2006.

BIOGRAPHY

Daniel Berkenstock *is a Ph.D candidate in Aeronautics and Astronautics at Stanford, working in the Stanford Aerospace Design Laboratory. Dan received the B.S.E in Aerospace Engineering at the University of Michigan, Ann Arbor, as well as the M.S. in Aeronautics and Astronautics at Stanford University. Dan's research combines the fields of aerospace-focused Multidisciplinary Shape Optimization with Convex Optimization. He has worked previously at Johnson Space Center, Ames Research Center, and Lawrence Livermore National Laboratory and co-founded the satellite imagery provider Skybox Imaging.*

Juan Alonso *is the founder and director of the Stanford Aerospace Design Laboratory (ADL) where he specializes in the development of high-fidelity computational design methodologies to enable the creation of realizable and efficient aerospace systems. His research involves a large number of different manned and unmannned applications including transonic, supersonic, and hypersonic aircraft, helicopters, turbomachinery, and launch and re-entry vehicles. He is the author of over 200 technical publications on the topics of computational aircraft and spacecraft design, multi-disciplinary optimization, fundamental numerical methods, and high-performance parallel computing.*

Laurent Lessard *is an Associate Professor of Mechanical and Industrial Engineering at Northeastern University, with courtesy appointments in ECE and CS. Before joining Northeastern, Laurent was a Charles Ringrose Assistant Professor of Electrical and Computer Engineering at the University of Wisconsin–Madison and a Faculty Member at the Wisconsin Institute for Discovery. Laurent received the B.A.Sc. in Engineering Science from the University of Toronto, and received the M.S. and Ph.D. in Aeronautics and Astronautics at Stanford University, advised by Sanjay Lall and co-advised by Matthew West. His research interests include: decentralized control, robust control, optimization, and machine learning.*

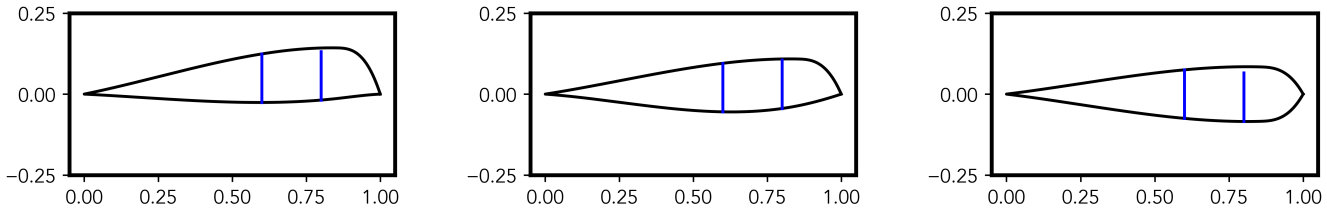

(a) $\gamma = 0.0$ - prioritized rcs reduction (b) $\gamma = 0.5$ - equally prioritized rcs and drag (c) $\gamma = 1.0$ - prioritized drag reduction

Figure 15. Optimal vehicle cross sections (minimum thickness constraint, shown) for varying γ ($\theta = 5°$, $\alpha = 0°$).

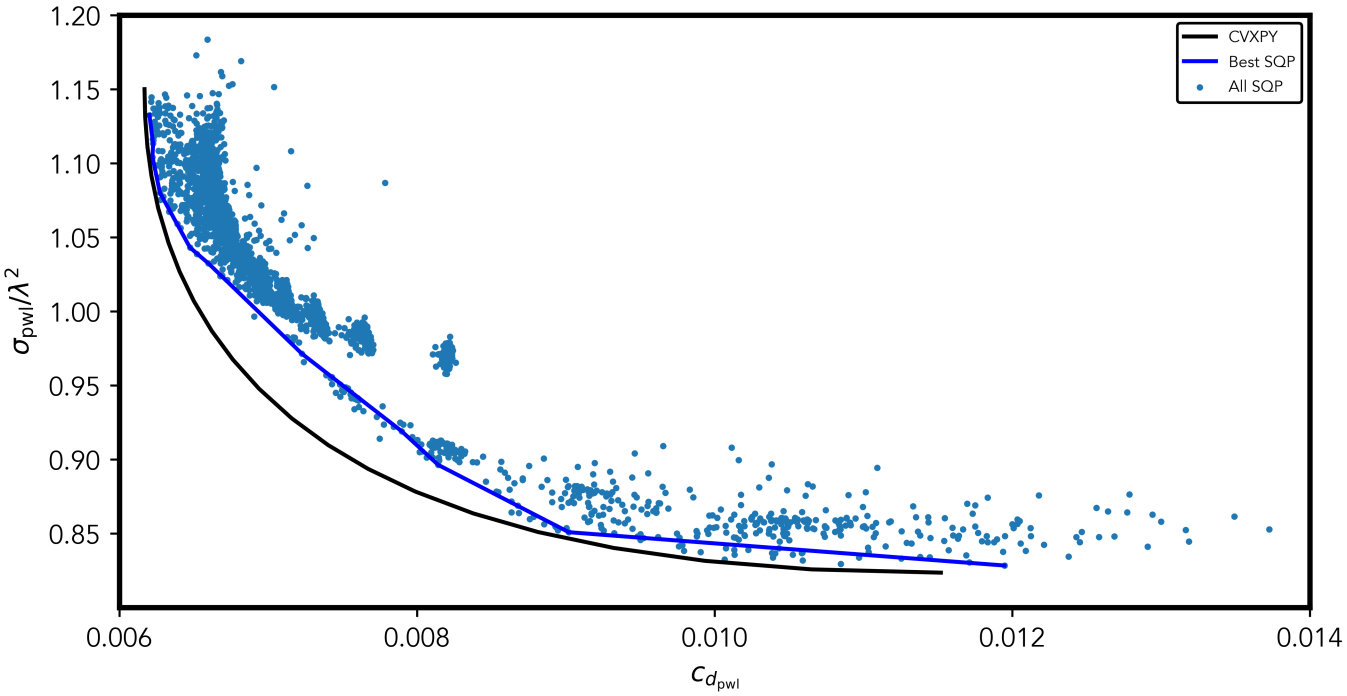

Figure 16. **Optimal results: CVXPY vx SQP,** $h = 6 \times 10^{-6}$**.**

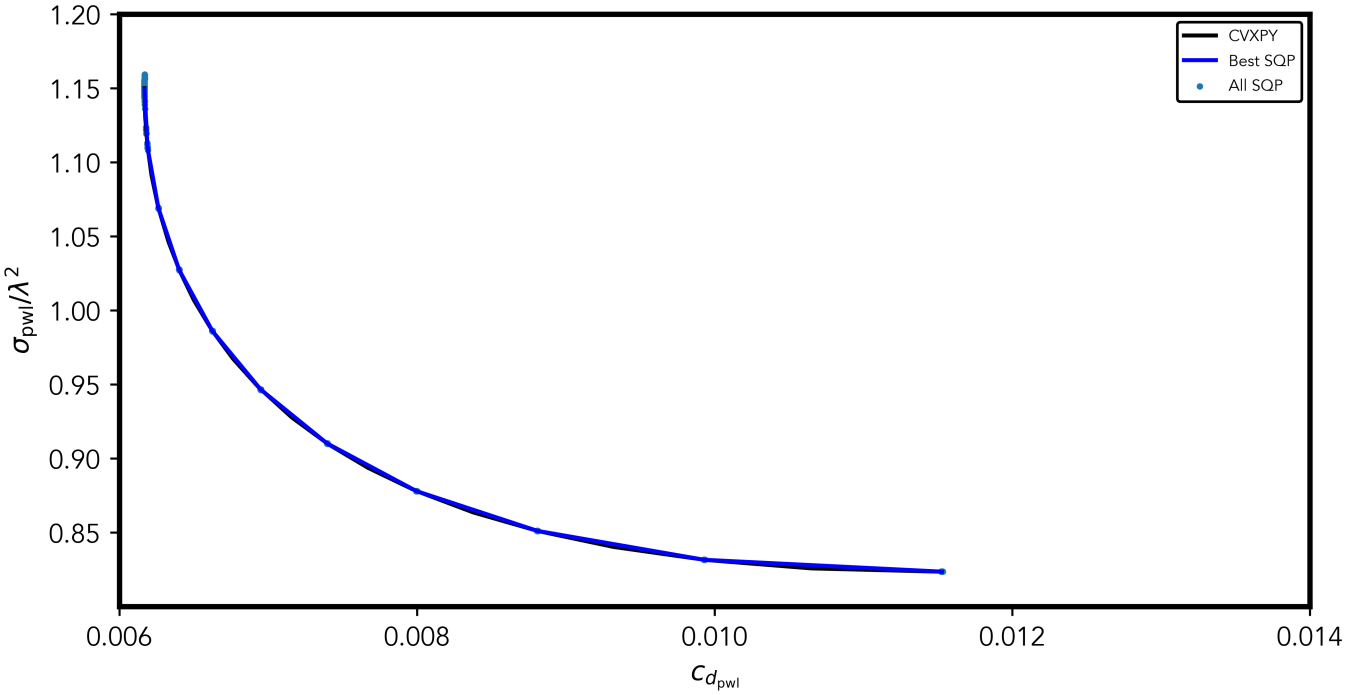

Figure 17. **Optimal results: CVXPY vx SQP,** $h = 5 \times 10^{-11}$.

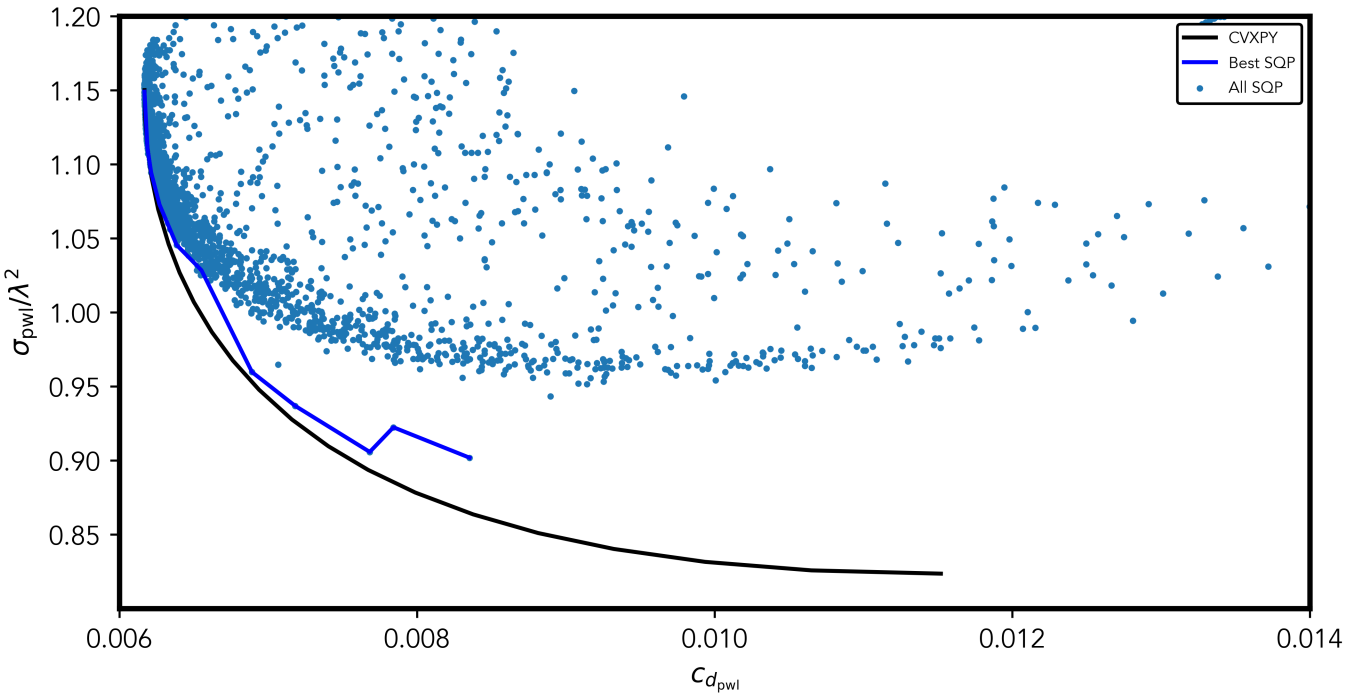

Figure 18. **Optimal results: CVXPY vx SQP,** $h = 5 \times 10^{-14}$.